Crossover and universality breaking in the dilute Baxter–Wu model

Accepted for publication in Physical Review E: Statistical, Nonlinear, and Soft Matter Physics

Crossover and universality breaking in the dilute Baxter–Wu model

Dimitrios Mataragkas,[1] Alexandros Vasilopoulos,[1,*] Dong-Hee Kim,[2,†] and Nikolaos G. Fytas[1,‡]

[1]*School of Mathematics, Statistics and Actuarial Science, University of Essex, Colchester CO4 3SQ, United Kingdom*

[2]*Department of Physics and Photon Science, Gwangju Institute of Science and Technology, Gwangju 61005, Republic of Korea*

(Dated: May 13, 2026)

The critical behavior of the Baxter-Wu model belongs to the universality class of the four-state Potts model. While the introduction of annealed vacancies does not alter the criticality of the four-state Potts model, the dilute Baxter-Wu model has remained the subject of several competing scenarios. Here we investigate the phase diagram of the spin-1 Baxter-Wu model in the presence of a crystal field using transfer-matrix calculations and large-scale Monte Carlo simulations. Our results provide strong evidence for continuously varying critical exponents at finite dilution and reveal a crossover to first-order behavior. Along the line of continuous transitions, the central charge remains close to $c = 1$, while the scaling dimensions systematically deviate from the spin-1/2 limit as the crystal field increases, eventually giving way to a first-order regime at strong fields. These findings resolve previous ambiguities and establish a consistent picture of the critical behavior of the dilute spin-1 Baxter-Wu model.

The Baxter-Wu model occupies a special place in statistical physics as a rare example of a two-dimensional spin system with multispin interactions and broken spin-inversion symmetry [1] that is nevertheless exactly solvable [2, 3]. Defined on the triangular lattice with three-spin ferromagnetic interactions (see Appendix A), the spin-1/2 Baxter-Wu model exhibits a four-fold degenerate ordered phase and a continuous phase transition with non-Ising critical exponents. Its critical behavior is described by a conformal field theory with central charge $c = 1$ and belongs to the universality class of the four-state Potts model [4], albeit without the logarithmic corrections present in the latter [5, 6].

A natural generalization introduces a crystal field (or single-ion anisotropy) coupling Δ and allows for a nonmagnetic state, leading to the spin-1 (or dilute) Baxter-Wu model. The Hamiltonian reads

$$\mathcal{H} = -J \sum_{\langle xyz \rangle} \sigma_x \sigma_y \sigma_z + \Delta \sum_x \sigma_x^2 = E_J + \Delta E_\Delta, \quad (1)$$

where $\sigma_i = \{-1, 0, 1\}$, the sum extends over all elementary triangles of the triangular lattice, and E_J and E_Δ the contributions of the exchange and the crystal field, respectively, to the total energy. Despite its apparent simplicity, this model is not exactly solvable and displays a rich phase diagram in the crystal-field–temperature (Δ, T) plane, including both continuous and first-order transition regimes, that have not been fully clarified [7, 8]. A sketch of the phase diagram is presented in the main panel of Fig. 1—see also Appendix B.

Based on analogies with diluted Potts models [9] and supporting numerical evidence, the existence of a multicritical point at finite values of Δ has long been conjectured [10]. However, both its location and even its nature remain unsettled [7, 8, 11], with additional conflicting scenarios regarding universality and other transition characteristics being reported in the literature [8, 12, 13]. In Ref. [7], the location of a pentacritical point was estimated as $(\Delta_{\rm pp}, T_{\rm pp}) \approx (0.8902, 1.4)$, whereas Ref. [8] proposed the substantially different values $(\Delta_{\rm pp}, T_{\rm pp}) \approx [1.68288(62), 0.98030(10)]$. If present, this pentacritical point corresponds to the coexistence of three ferrimagnetic configurations, a ferromagnetic configuration, and the zero-spin state. Furthermore, the validity of universality along the continuous transition line remains under debate [14–16], with proposals ranging from continuously varying critical exponents to four-state Potts behavior [8, 12, 13]. With respect to the first-order transition regime, to the best of our knowledge no relevant study currently exists.

We revisit this longstanding problem using complementary numerical and theoretical approaches. By combining transfer-matrix calculations, finite-size scaling, and large-scale Monte Carlo simulations, we systematically explore the phase transitions of the dilute spin-1 Baxter–Wu model across the (Δ, T) phase diagram. We demonstrate that the system exhibits a line of continuous transitions extending up to a broad crossover regime, with no evidence for a multicritical point. Along this line, central-charge estimates remain close to $c \simeq 1$, while both transfer-matrix and Monte Carlo analyses reveal a systematic variation of effective critical exponents away from the four-state Potts values [4] that becomes increasingly pronounced as the crossover regime is approached. In the intermediate regime, previously conjectured to host a multicritical point, we instead identify pronounced crossover behavior marked by a drift of effective conformal properties, signaling the breakdown of conformal and scale invariance. The system thus evolves from second-order criticality to first-order behavior through an extended crossover region rather than via a higher-order singular point. Finally, in the low-T (or large-Δ) regime,

* alex.vasilopoulos@essex.ac.uk
† dongheekim@gist.ac.kr
‡ nikolaos.fytas@essex.ac.uk

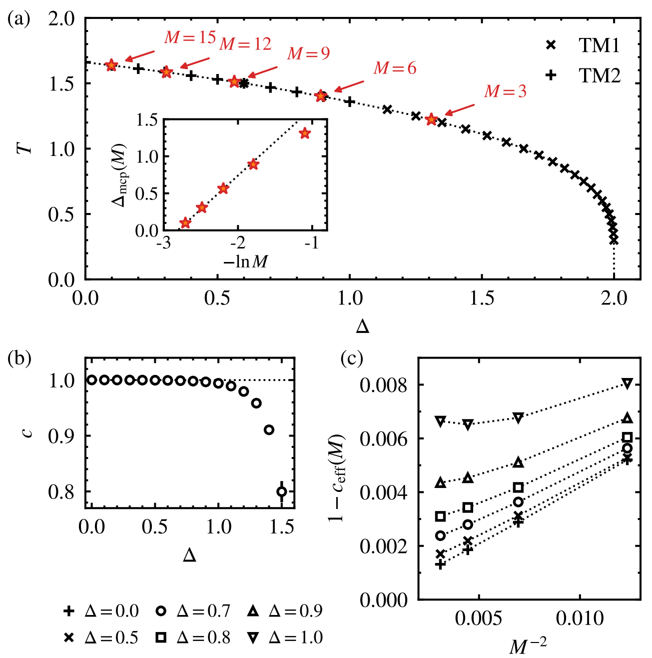

FIG. 1. Phase diagram of the spin-1 Baxter-Wu model. (a) Transition points in the (Δ, T) plane, shown for $\Delta \geq 0$. The labels TM1 and TM2 denote the transitions points located using the ansatz for the first-order and second-order transitions, respectively. Stars indicate the heuristic test for a multicritical point proposed in Ref. [7], based on size triplets $(M, M+3, M+6)$. (b) Central charge c estimated along the transition line. (c) Finite-size behavior of the effective central charge for $M \geq 9$. Dotted lines serve as guides to the eye.

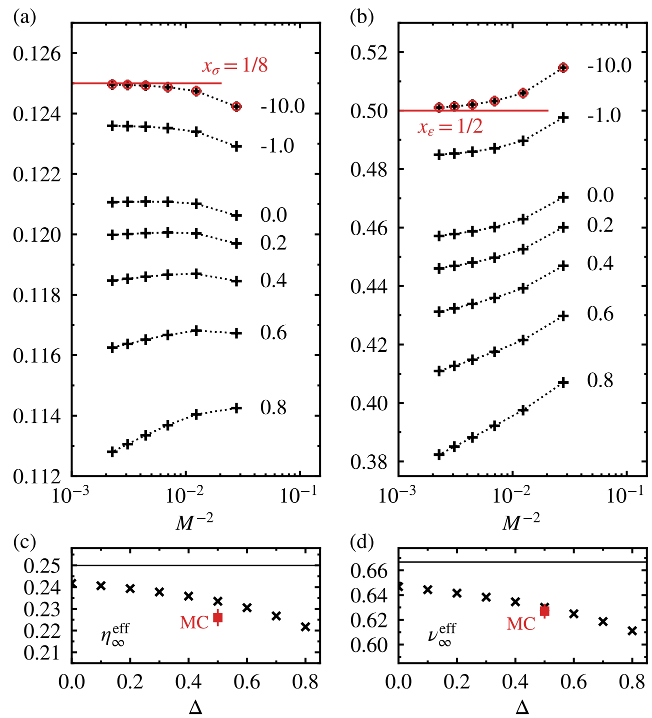

FIG. 2. Scaling dimensions with increasing dilution. Finite-size behavior of the effective scaling dimensions $x_1^{\rm eff}$ (a) and $x_4^{\rm eff}$ (b) for several values of Δ indicated in the panels. Open circles denote results for the spin-1/2 model. The corresponding effective critical exponents (c) $\eta^{\rm eff}$ and (d) $\nu^{\rm eff}$ extrapolated to $M = \infty$ are compared with Monte Carlo (MC) estimates at $\Delta = 0.5$ (red squares). Solid lines indicate the exact values of the four-state Potts universality class, $\eta = 1/4$ and $\nu = 2/3$.

we establish that the transition is unequivocally first order, characterized by double-peaked energy distributions and an interfacial tension that increases upon cooling.

In the limit $\Delta = -\infty$, the spin-1 model reduces to the spin-1/2 Baxter-Wu model. Within conformal field theory [5], the spectrum on an infinite strip of finite width M with periodic boundary conditions is described by

$$\epsilon_\alpha(M) = \epsilon_\infty + \frac{2\pi v_s}{M^2}\left(x_\alpha - \frac{c}{12} + R_\alpha(M)\right), \qquad (2)$$

where $\epsilon_\alpha = -(\ln \lambda_\alpha)/M$ is the energy associated with the transfer-matrix eigenvalue λ_α. The central charge c and the scaling dimensions x_α can be estimated by analyzing the finite-size behavior of the spectrum. In particular, the effective central charge is obtained from the ground-state energies as

$$c_{\rm eff}(M) = \frac{6}{\pi v_s}\frac{\epsilon_0(M+3) - \epsilon_0(M)}{M^{-2} - (M+3)^{-2}}, \qquad (3)$$

where the ground state corresponds to $x_0 = 0$. Similarly, the effective scaling dimensions are given as

$$x_\alpha^{\rm eff}(M) = \frac{1}{2\pi v_s} M \ln \frac{\lambda_0}{\lambda_\alpha}, \qquad (4)$$

whose convergence is governed by the finite-size corrections $R_\alpha(M)$. It is well established that the spin-1/2 model belongs to the four-state Potts universality class [4], characterized by a central charge $c = 1$ and scaling dimensions $x_\alpha \in \{0, 1/8, 1/2, \ldots\}$. However, the finite-size corrections differ: for the spin-1/2 Baxter-Wu model they scale as $R_\alpha(M) \sim M^{-2}$, in contrast to the logarithmic corrections expected for the four-state Potts model [5].

A possible scenario for finite Δ is that the critical exponents vary continuously along the critical line until it meets the first-order region at a multicritical point, as suggested by early transfer-matrix calculations for $M \leq 9$ [10]. We revisit this scenario by extending the calculations up to $M = 21$ (see Appendix C 1), employing sparse-matrix factorization in the geometry with $v_s = \sqrt{3}$ [17]. The largest five eigenvalues $(\lambda_{0,1,2,3,4})$ are computed using the thick-restart Lanczos algorithm, allowing us to track the effective central charge $c_{\rm eff}$ and the effective scaling dimensions $x_1^{\rm eff}$ and $x_4^{\rm eff}$. Here $\lambda_{1,2,3}$ are degenerate by symmetry, which requires M to be a multiple of 3. Transition points (see Appendix C 2) are determined from the crossing of the scaled correlation length $\propto 1/x_1^{\rm eff}$ [7, 18], as well as from the minimum of $x_4^{\rm eff}$, which signals an avoided spectral crossing [17, 18]. Although these criteria are typically associated with second- and first-order transitions, respectively, they yield consistent estimates within the crossover region shown in Fig. 1(a).

In estimating the central charge, we find that extrapolations of $c_{\rm eff}$ using data for $M \geq 9$ yield values very close to $c = 1$ for $\Delta \lesssim 0.5$. For example, at $\Delta = 0.5$ we obtain $c = 0.9997(1)$, after which the estimates gradually decrease, as shown in Fig. 1(b). Determining the precise endpoint of the critical line with $c = 1$ remains challenging. However, the finite-size behavior of $c_{\rm eff}$ in Fig. 1(c) reveals a systematic deviation from the expected correction $R_0 \sim M^{-2}$ as Δ increases across the crossover region. In particular, the pronounced curvature observed at $\Delta = 1$ signals a clear departure from $c = 1$, consistent with the onset of first-order behavior.

However, observing $c = 1$ alone does not guarantee that the critical line of the dilute spin-1 model belongs to the same universality class as the spin-1/2 limit unless the operator content is also verified. In particular, there is no clear evidence that the scaling dimensions recover those of the spin-1/2 model at finite Δ. Figure 2 shows that the effective scaling dimensions $x_1^{\rm eff}$ and $x_4^{\rm eff}$ drift systematically away from the spin-1/2 values $x_\sigma = 1/8$ and $x_\epsilon = 1/2$ as Δ increases. Notably, for a fixed Δ, the estimate of $x_4^{\rm eff}$ moves even farther from the spin-1/2 line as the strip width M increases, indicating that the deviation in x_4 is not a finite-size artifact. Although the accessible range of M remains limited in transfer-matrix calculations, the observed systematic drift of the scaling dimensions suggests that the critical exponents may vary continuously with Δ. Consequently, the critical line away from the $\Delta = -\infty$ limit may not belong to the universality class of the four-state Potts model.

To estimate the effective critical exponents, $\eta^{\rm eff} \equiv 2x_1^{\rm eff}$ and $\nu^{\rm eff} \equiv (2 - x_4^{\rm eff})^{-1}$, we extrapolate the effective scaling dimensions to the limit $M \to \infty$ by assuming the finite-size correction

$$R_\alpha(M) \simeq a_\alpha M^{-1} + b_\alpha M^{-2}, \tag{5}$$

where the M^{-2} term is inherited from the spin-1/2 limit. The additional M^{-1} contribution is introduced to capture the pronounced curvature of $x_1^{\rm eff}$ for $\Delta \gtrsim 0$, which may also explain the inconclusive search for a multicritical point based on a plateau of $x_1^{\rm eff}$ as a heuristic indicator [7]. As illustrated in Fig. 2(a), increasing M in the size-triplet test systematically shifts the apparent plateau toward smaller Δ. This behavior can be interpreted in terms of the drift of the zero-slope point $M = -2b/a$ of $R_\alpha(M)$. The ratio $|a/b|$ decreases as Δ becomes more negative, recovering the expected scaling $R_\alpha(M) \propto M^{-2}$ in the limit $\Delta = -\infty$. For example, at $\Delta = -10$ we obtain $|a_1/b_1| < 10$ and $|a_4/b_4| < 50$, yielding $\eta_\infty^{\rm eff} = 0.24986(1)$ and $\nu_\infty^{\rm eff} = 0.66678(5)$, in excellent agreement with the exact 1/8 and 2/3 exponents of the spin-1/2 limit. The gradual evolution of the exponents is quantified by the extrapolations shown for $\Delta > 0$ in Fig. 2(c) and (d).

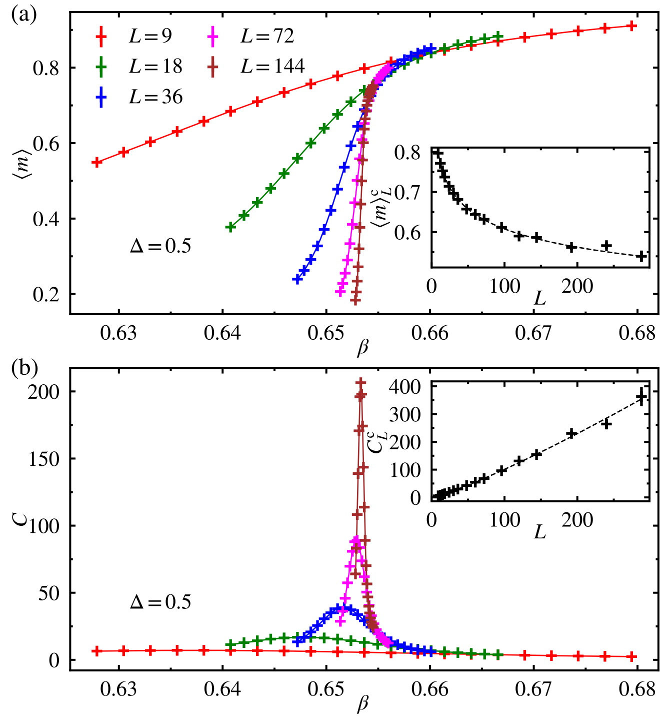

FIG. 3. (a) Order-parameter $\langle m\rangle$ and (b) specific-heat C (b) curves as functions of the inverse temperature ($\beta \equiv 1/T$) obtained from Monte Carlo simulations. Representative system sizes are indicated in the panels. Insets show the corresponding finite-size scaling at the critical point for $\Delta = 0.5$.

A remaining question concerns the location in the phase diagram where the second-order transition terminates and first-order behavior sets in. While the departure from $c = 1$ observed in Fig. 1(c) suggests that this endpoint lies below $\Delta = 1$, the resolution of the transfer-matrix calculations is limited by the accessible strip widths M. It is instructive to contrast this behavior with the Blume–Capel model, where the tricritical point is characterized by a distinct set of central charge and scaling dimensions, enabling precise finite-size scaling analyses via the persistence length [17]. In addition, the finite-size correction of $x_1^{\rm eff}$ in the Blume–Capel model exhibits a sharp sign change across the first- and second-order regimes, making the heuristic plateau test particularly effective. By contrast, the transfer-matrix spectrum of the spin-1 Baxter–Wu model does not display similarly distinct multicritical signatures. This lack of clear spectral indicators motivates the use of reciprocal numerical approaches to determine the onset of first-order behavior.

To enhance the transfer-matrix analysis within the continuous transition regime we perform large-scale Monte Carlo simulations at $\Delta = 0.5$ for systems with linear sizes $L = \in \{9 - 288\}$. For details of the numerical implementation we refer to Appendix D. Typical order-parameter ($\langle m\rangle$) and specific-heat (C) curves for representative system sizes are shown in the main panels

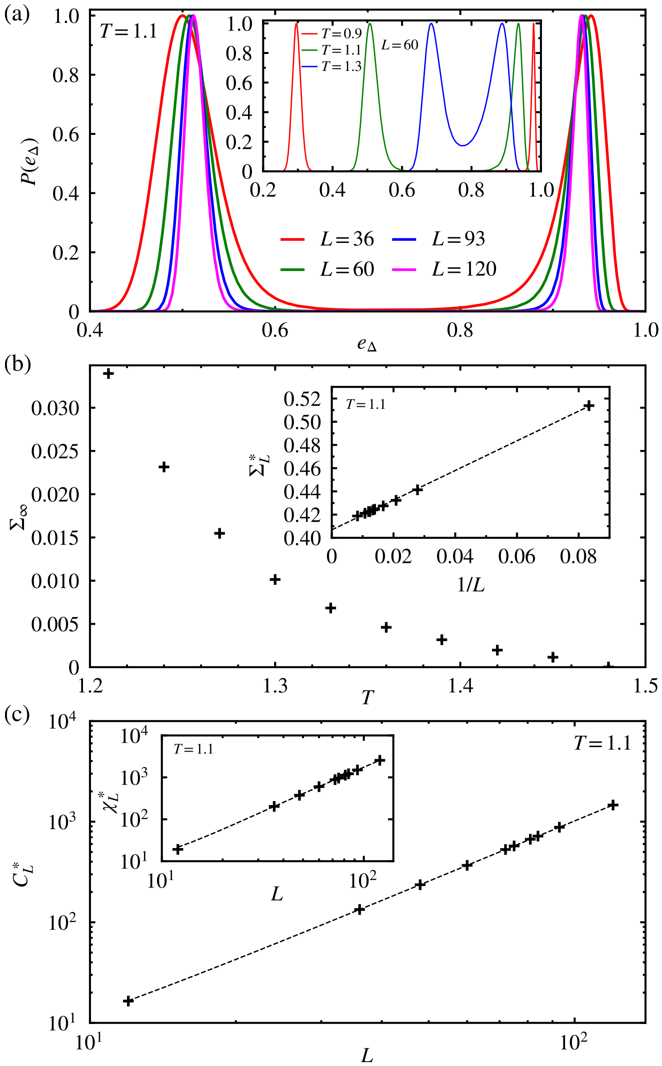

FIG. 4. (a) Multicanonical probability density functions $P(e_\Delta)$ for a wide range of system sizes at $T = 1.1$ (main panel) and for selected temperatures at fixed $L = 60$ (inset), illustrating phase coexistence and the rapid growth of the free-energy barrier upon lowering the temperature. (b) Interfacial tension Σ_∞ as a function of temperature T, indicating the onset of the first-order regime near $T \approx 1.42$ ($\Delta \approx 0.84$). The apparent approach of Σ_∞ to zero extends into the second-order region due to finite-size effects associated with the persistent double-peaked energy distribution [14]. The inset shows a typical extrapolation yielding $\Sigma_\infty \approx 0.41$ at $T = 1.1$, about an order of magnitude larger than the values in the main panel, indicating an exponential increase of Σ_∞ as $T \to 0$. (c) Finite-size scaling of the maxima of the specific heat (main panel) and magnetic susceptibility (inset), consistent with the expected $\sim L^d$ scaling for a first-order transition in $d = 2$.

of Fig. 3. The insets display the corresponding finite-size scaling behavior at the critical point $\beta_c = 0.653562$ for $\Delta = 0.5$ [15], following the forms $\langle m\rangle_L^c = b_m L^{-\beta/\nu}$ and $C_L^c = b_C L^{\alpha/\nu}$, where $\{b_m, b_C\}$ are non-universal amplitudes. From the scaling of the order parameter [Fig. 3(a)] we obtain $\eta = 0.226(4)$ via the Fisher scaling relation [19], $\eta = 2(\beta/\nu) - (d-2)$. The analysis of the specific heat [Fig. 3(b)] yields $\alpha/\nu = 1.188(5)$, which in turn gives $\nu = 2/(d + \alpha/\nu) = 0.627(3)$ through the hyperscaling relation. The Monte Carlo estimates of η and ν closely track the transfer-matrix effective exponents [see Fig. 2(c) and (d)], differ clearly from the four-state Potts values $\eta = 1/4$ and $\nu = 2/3$, and support the breaking of universality through a systematic variation of the critical behavior along the transition line. This contrasts sharply with the Blume–Capel ferromagnet [20, 21], where universality remains robust along the second-order transition line.

To probe now the remaining first-order transition regime of the phase boundary, emerging at $\Delta \gtrsim 0.85$ ($T \lesssim 1.42$) [Fig. 4(b)], we implement multicanonical simulations [22] which efficiently sample configurations separated by large free-energy barriers. In this approach, the Boltzmann weight associated with the crystal-field energy E_Δ is replaced by a generalized weight $W(E_\Delta)$ chosen to produce a flat histogram in E_Δ. For the spin-1 Baxter-Wu model, whose density of states depends on two energies $\Gamma(E_J, E_\Delta)$, the multicanonical scheme is applied to E_Δ, allowing unrestricted reweighting in the crystal field Δ at fixed temperature [23]. The corresponding partition function reads $\mathcal{Z}_{\mathrm{MUCA}} = \sum_{E_J,E_\Delta} \Gamma(E_J, E_\Delta)\, e^{-\beta E_J}\, W(E_\Delta)$. Once the weights are determined, canonical observables at arbitrary Δ follow from standard reweighting [24]. This framework enables direct estimates of the normalized probability density functions $P(e_\Delta)$ ($e_\Delta = E_\Delta/L^2$), free-energy barriers, and thermodynamic response functions across the first-order line. In the following we consider system sizes $L \in \{12 - 120\}$ for temperatures between $T = 1.45$ and $T = 1.1$. In finite systems, a double-peaked structure of $P(e_\Delta)$ signals the phase coexistence characteristic of a first-order transition [25, 26]. Representative distributions at $T = 1.1$ are shown in Fig. 4(a) for a wide range of system sizes and display a pronounced suppression of intermediate states. The inset presents $P(e_\Delta)$ at selected temperatures for fixed $L = 60$, illustrating the rapid growth of the free-energy barrier upon lowering the temperature. These features provide clear and direct evidence of first-order behavior. From equal-height (eqh) distributions, we extract the free-energy barrier separating the coexisting phases [27, 28], $\Delta F_L = \frac{1}{2\beta\Delta} \ln\left[(P_{\max}/P_{\min})_{\mathrm{eqh}}\right]$, where $P_{\max}$ and $P_{\min}$ denote the peak value and the intervening minimum of $P(e_\Delta)$, respectively. The corresponding interfacial tension, $\Sigma_L = \Delta F_L/L$, is expected in two dimensions to scale as $\Sigma_L = \Sigma_\infty + c_1 L^{-1} + \mathcal{O}(L^{-2})$ (see the inset of Fig. 4(b) for a common extrapolation to a nonzero value $\Sigma_\infty = 0.407(1)$ at $T = 1.1$). Overall, the interfacial tension increases monotonically upon lowering the temperature, as shown in the main panel of Fig. 4(b), consistent with earlier studies of the analogous triangular Blume-Capel ferromagnet [17, 29], although the increase is much more pronounced in the present Baxter-Wu case. Additional confirmation is provided by the scaling of thermodynamic response functions. At a first-order transition, the maxima of the specific heat and susceptibility are expected to scale with the volume, with corrections in inverse powers of the volume [20, 23, 25, 30, 31]. Accordingly, we fit the full set of data using $C_L^* = b_C L^x(1 + b_C' L^{-2})$, and $\chi_L^* = b_\chi L^x(1 + b_\chi' L^{-2})$, where $\{b_C, b_C', b_\chi, b_\chi'\}$ are non-universal amplitudes, as above. As shown in Fig. 4(c), this Ansatz provides excellent fits for both observables, providing $x = 2.000(5)$ for the specific heat and $x = 2.004(4)$ for the susceptibility, in perfect agreement with the expected value $d = 2$.

In summary, our combined transfer-matrix and Monte Carlo analysis provides a coherent picture of the phase behavior of the dilute spin-1 Baxter–Wu model in the presence of a crystal field. We find that the continuous transition line emerging from the spin-1/2 limit does not terminate at a multicritical point. Instead, it extends into a broad crossover regime in which the critical properties progressively depart from those of the four-state Potts universality class. In this region, the effective scaling behavior and conformal signatures gradually lose stability, signaling the onset of nonuniversal behavior. Upon further lowering the temperature or increasing the crystal field, the system ultimately enters a regime of genuine first-order transitions characterized by phase coexistence and finite interfacial tension. Taken together, these results resolve previous ambiguities regarding the phase diagram of the dilute Baxter-Wu model and demonstrate how multispin interactions and the associated degeneracy structure can destabilize universality, leading to a broad crossover between continuous and first-order transitions.

ACKNOWLEDGMENTS

N.G. F. would like to thank J.A. Plascak for his ongoing collaboration on the problem and the many fruitful discussions over the last years. Part of the numerical calculations reported in this paper were performed at the High-Performance Computing cluster CERES of the University of Essex. The work of A. V. and N.G. F. was supported by the Engineering and Physical Sciences Research Council (grant EP/X026116/1 is acknowledged).

Appendix A: The original spin-1/2 Baxter-Wu model

The pure spin-1/2 Baxter-Wu model is defined on the triangular lattice by the Hamiltonian

$$\mathcal{H} = -J \sum_{\langle xyz \rangle} \sigma_x \sigma_y \sigma_z, \tag{A1}$$

where the exchange interaction $J > 0$, the sum runs over all elementary triangles of a lattice with N sites, and $\sigma_x = \pm 1$ are Ising spin-1/2 variables. The triangular lattice can be partitioned into three sublattices, A, B, and C, as illustrated in Fig. 5, such that each triangular face contains exactly one site from each sublattice. The ground state of the model is four-fold degenerate: one ferromagnetic configuration with all spins aligned and three ferrimagnetic configurations in which two sublattices carry spins pointing down and the remaining one spins pointing up. The Hamiltonian in Eq. (A1) is also self-dual [1, 32], yielding the same critical temperature as the spin-1/2 Ising model on the square lattice, $k_{\rm B}T_{\rm c}/J = 2/\ln(1+\sqrt{2}) = 2.269185\ldots$, where $k_{\rm B}$ denotes the Boltzmann constant.

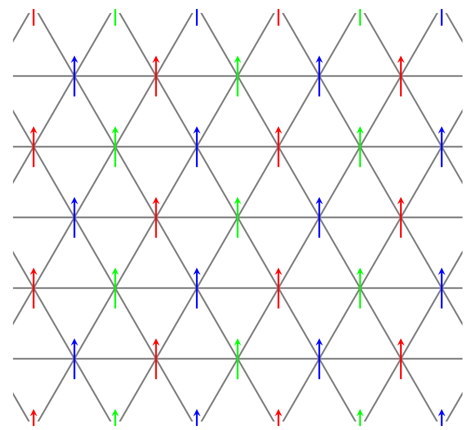

FIG. 5. Representation of the Baxter-Wu triangular lattice as a superposition of the three sublattices, A, B, and C. Each sublattice corresponds to spins of a different color. The spins are shown in the ferromagnetic ground state.

Appendix B: Phase diagram transition points of the spin-1 Baxter-Wu model

In Tab. I below we provide a summary of transition and critical points corresponding to the phase diagram of the spin-1 Baxter-Wu model, as well as estimates of the critical exponents η and ν.

Appendix C: Transfer-matrix method

In this section, we provide the details of the transfer-matrix implementation and the procedures to identify the transitions points.

1. Sparse-matrix factorization

We construct the transfer matrix $\mathbf{T}$ in the two-layer geometry of the triangular lattice following the sparse-matrix factorization introduced in Ref. [17]. We adopt the same convention for labeling sites in the strip geometry illustrated in Fig. 2 of Ref. [17], except that here

TABLE I. Transition points and critical exponents of the spin-1 Baxter-Wu model identified in the present work. The transition points obtained from transfer-matrix calculations are determined by extrapolation assuming first-order (TM1) and second-order (TM2) scaling forms. Results from multicanonical (MUCA) simulations are listed in the third column. The last two columns report the estimates of the critical exponents η and ν extracted from the transfer-matrix spectrum.

T	Δ^*_∞ (TM1)	Δ^*_∞/Δ_c (MUCA)	Δ	T_c (TM2)	$\eta^{\mathrm{eff}}_\infty$	$\nu^{\mathrm{eff}}_\infty$
0.30	1.999 236					
0.35	1.997 686					
0.40	1.994 580					
0.45	1.989 318					
0.50	1.981 347					
0.55	1.970 175					
0.60	1.955 361					
0.65	1.936 497					
0.70	1.913 193					
0.75	1.885 062					
0.80	1.851 714					
0.85	1.812 755					
0.90	1.767 781					
0.95	1.716 384					
1.00	1.658 160					
1.05	1.592 709					
1.10	1.519 634	1.519 66(2)				
1.15	1.438 523					
1.20	1.348 935					
1.25	1.250 375					
1.30	1.142 281					
			1.0	1.359 662		
			0.9	1.398 081	0.2150(3)	0.602(2)
1.40	0.894 766					
			0.8	1.434 077	0.2217(2)	0.611(1)
			0.7	1.467 937	0.2267(1)	0.618(1)
			0.6	1.499 896	0.230 53(6)	0.6249(8)
1.50	0.599 658					
1.5301		0.4999(2)				
			0.5	1.530 149	0.233 50(3)	0.6301(6)
			0.4	1.558 856	0.235 86(2)	0.6345(5)
			0.3	1.586 152	0.237 77(1)	0.6383(4)
			0.2	1.612 155	0.239 34(1)	0.6416(3)
			0.1	1.636 964	0.240 65(1)	0.6443(2)
1.6606		0.0008(7)				
			0.0	1.660 667	0.241 75(1)	0.6468(2)
			−1.0	1.850 262	0.247 11(1)	0.659 55(7)
			−10.0	2.257 751	0.249 86(1)	0.666 78(5)

M denotes the strip width, to avoid confusion with the linear system size L used in the Monte Carlo simulations on $L \times L$ lattices.

The transfer matrix can be written in the factorized form

$$\mathbf{T} = \mathbf{R}\left(\mathbf{V}^{1/2}\mathbf{T}_M\mathbf{T}_{M-1}\cdots\mathbf{T}_2\mathbf{T}_1\mathbf{V}^{1/2}\right)^2, \qquad \text{(C1)}$$

where $\mathbf{V}$ is a diagonal matrix with elements

$$\langle \mathbf{s}|\mathbf{V}|\mathbf{s}'\rangle = \exp\left[-\beta\Delta\sum_{j=1}^{M} s_j^2\right]\prod_{j=1}^{M}\delta_{s_j,s'_j}. \qquad \text{(C2)}$$

The matrix elements of $\mathbf{T}_1$, $\mathbf{T}_k$ $(k = 2,\ldots,M-1)$, and $\mathbf{T}_M$ are given by

$$\langle \mathbf{s}|\mathbf{T}_1|\mathbf{s}'\rangle = \exp[\beta J s_1 s_1' s_2']\ \delta_{s_{M+1},s_1'} \prod_{j=2}^{M} \delta_{s_j,s_j'}, \tag{C3}$$

$$\langle \mathbf{s}|\mathbf{T}_k|\mathbf{s}'\rangle = \exp\big[\beta J s_k s_k'(s_{k-1} + s_{k+1}')\big] \prod_{j=1}^{k-1} \delta_{s_j,s_j'} \prod_{j=k+1}^{M+1} \delta_{s_j,s_j'}, \tag{C4}$$

$$\langle \mathbf{s}|\mathbf{T}_M|\mathbf{s}'\rangle = \exp\big[\beta J s_M(s_{M-1}s_M' + s_M' s_{M+1}' + s_1 s_{M+1}')\big] \prod_{j=1}^{M-1} \delta_{s_j,s_j'}, \tag{C5}$$

respectively. In the final step, $\mathbf{R}$ denotes a cyclic rotation operator acting on the site indices, which restores the symmetry of the transfer matrix.

To obtain the leading part of the spectrum, we employ the thick-restart Lanczos algorithm and compute the five largest eigenvalues. The sparse factorization enables transfer-matrix calculations for strip widths up to $M = 21$ within our available computational resources.

2. Transition points

The transition points are determined using two complementary approaches. Assuming a second-order transition for fixed $\Delta \le 1$, we locate the crossing point $T_{M,M+3}$ of the scaled correlation length, $\xi_M/M \equiv [M \ln(\lambda_0/\lambda_1)]^{-1}$, between strips of widths M and $M+3$. Since the scaled correlation length is inversely proportional to the effective scaling dimension x_1^{eff}, its finite-size behavior at the critical point can be written using the same correction form $R(M)$ assumed for the scaling dimensions,

$$\xi_M(T_\mathrm{c}) = A_0 M \left(1 + \frac{A_1}{M} + \frac{A_2}{M^2} + \cdots\right), \tag{C6}$$

$$\left(\frac{\mathrm{d}\xi_M}{\mathrm{d}T}\right)_{T_\mathrm{c}} = B_0 M^{1+y} \left(1 + \frac{B_1}{M} + \frac{B_2}{M^2} + \cdots\right). \tag{C7}$$

Using these Ansätze, the crossing temperatures can be extrapolated according to

$$T_{M,M+3} = T_\mathrm{c} + M^{-y}(aM^{-1} + bM^{-2}), \tag{C8}$$

where we treat $y = 1/\nu + \tilde{\omega}$ as a free parameter (see Ref. [18] and references therein for details). In the fits we exclude the data point for $M = 6$. The resulting estimates of the critical temperatures for $\Delta = (-10, -1, 0, 0.5)$ are $T_\mathrm{c} = (2.257751, 1.850262, 1.660667, 1.530149)$, in excellent agreement with the Monte Carlo estimates reported in Table I of Ref. [15].

Assuming instead a first-order transition for fixed $T \le 1.5$, we locate the transition point by extrapolating the value Δ_M that minimizes the spectral gap between ϵ_0 and ϵ_4, corresponding to the effective scaling dimension $x_4^{\mathrm{eff}}(M)$. As discussed for the Blume-Capel model in Refs. [17, 18], the sequence Δ_M converges exponentially with increasing M near an avoided spectral crossing, providing a clear signature of a first-order transition. Finite-size effects become stronger as T approaches the continuous-transition regime, where we instead employ an empirical power-law extrapolation to estimate the transition point. Despite relying on different assumptions about the nature of the transition, the resulting estimates fall on the same curve within the crossover region.

Appendix D: Monte Carlo simulations

Our Monte Carlo simulations employ Metropolis sampling combined with histogram reweighting [33]. For each system size within $L = 9 - 288$ an average over 100 independent realizations is performed to increase statistical accuracy. All runs are carried out in reduced units ($J = 1$, $k_\mathrm{B} = 1$) on triangular lattices with periodic boundary conditions. To accommodate both the ferromagnetic ground state and the three ferrimagnetic configurations, the linear system size L is restricted to multiples of three [13]. The sampled observables include estimates of the mean energy $\langle E\rangle$, the order parameter $\langle m\rangle$ which is estimated from the root mean square average of the magnetization per site of the three sublattices A, B, and C [12, 13, 34]

$$m = \sqrt{\frac{m_\mathrm{A}^2 + m_\mathrm{B}^2 + m_\mathrm{C}^2}{3}}, \tag{D1}$$

and the specific heat

$$C = \left[\langle E^2\rangle - \langle E\rangle^2\right]/(LT)^2. \tag{D2}$$

Finally, for all scaling analyses, fits are performed using data with $L \ge L_\mathrm{min}$, and their quality was assessed using the standard χ^2 goodness-of-fit test. In particular, fits are considered acceptable only when the quality-of-fit parameter satisfied $10\% < Q < 90\%$ [35].

[1] D. W. Wood and H. P. Griffiths, A self dual relation for an Ising model with triplet interactions, J. Phys. C: Solid State Phys. **5**, L253 (1972).

[2] R. J. Baxter and F. Y. Wu, Exact solution of an Ising model with three-spin interactions on a triangular lattice, Phys. Rev. Lett. **31**, 1294 (1973).

[3] R. J. Baxter, *Exactly Solved Models in Statistical Mechanics* (Academic Press, London, 1982).

[4] E. Domany and E. K. Riedel, Phase transitions in two-dimensional systems, Journal of Applied Physics **49**, 1315 (1978), https://pubs.aip.org/aip/jap/article-pdf/49/3/1315/18379074/1315_1_online.pdf.

[5] F. C. Alcaraz and J. C. Xavier, Conformal invariance studies of the Baxter-Wu model and a related site-colouring problem, J. Phys. A: Math. and Gen. **30**, L203 (1997).

[6] F. C. Alcaraz and J. C. Xavier, Critical and off-critical studies of the Baxter-Wu model with general toroidal boundary conditions, J. Phys. A: Math. and Gen. **32**, 2041 (1999).

[7] D. A. Dias, J. C. Xavier, and J. A. Plascak, Critical behavior of the spin-1 and spin-3/2 Baxter–Wu model in a crystal field, Phys. Rev. E **95**, 012103 (2017).

[8] L. N. Jorge, P. H. L. Martins, C. J. DaSilva, L. S. Ferreira, and A. A. Caparica, An entropic simulational study of the spin-1 Baxter–Wu model in a crystal field, Physica A **576**, 126071 (2021).

[9] B. Nienhuis, A. N. Berker, E. K. Riedel, and M. Schick, First- and Second-Order Phase Transitions in Potts Models: Renormalization-Group Solution, Phys. Rev. Lett. **43**, 737 (1979).

[10] M. L. M. Costa, J. C. Xavier, and J. A. Plascak, Phase diagram and critical behavior of the spin-1 Baxter-Wu model with a crystal field, Phys. Rev. B **69**, 104103 (2004).

[11] W. Kinzel, E. Domany, and A. Aharony, Finite size scaling analysis of the dilute baxter-wu model, J. Phys. A: Math. and Gen. **14**, L417 (1981).

[12] M. L. M. Costa and J. A. Plascak, Monte Carlo study of the spin-1 Baxter-Wu model, Braz. J. Phys. **34**, 419–421 (2004).

[13] M. L. M. Costa and J. A. Plascak, Monte Carlo study of the Spin-1 Baxter-Wu model in a crystal field, J. Phys.: Conf. Ser. **686**, 012011 (2016).

[14] A. Vasilopoulos, N. G. Fytas, E. Vatansever, A. Malakis, and M. Weigel, Universality in the two-dimensional dilute Baxter–Wu model, Phys. Rev. E **105**, 054143 (2022).

[15] A. R. S. Macêdo, A. Vasilopoulos, M. Akritidis, J. A. Plascak, N. G. Fytas, and M. Weigel, Two-dimensional dilute Baxter-Wu model: Transition order and universality, Phys. Rev. E **108**, 024140 (2023).

[16] A. R. S. Macêdo, J. A. Plascak, A. Vasilopoulos, N. G. Fytas, M. Akritidis, and M. Weigel, Universal energy and magnetisation distributions in the Blume–Capel and Baxter–Wu models, Journal of Statistical Mechanics: Theory and Experiment **2024**, 103204 (2024).

[17] D. Mataragkas, A. Vasilopoulos, N. G. Fytas, and D.-H. Kim, Transfer-matrix approach to the Blume-Capel model on the triangular lattice, Phys. Rev. Res. **7**, 033240 (2025).

[18] M. Jung and D.-H. Kim, First-order transitions and thermodynamic properties in the 2D Blume-Capel model: the transfer-matrix method revisited, Eur. Phys. J B **90**, 245 (2017).

[19] D. P. Landau and K. Binder, *A Guide to Monte Carlo Simulations in Statistical Physics*, 5th ed. (Cambridge University Press, Cambridge, 2021).

[20] J. Zierenberg, N. G. Fytas, M. Weigel, W. Janke, and A. Malakis, Scaling and universality in the phase diagram of the 2D Blume-Capel model, Eur. Phys. J. Spec. Top. **226**, 789 (2017).

[21] M. Blume, Theory of the First-Order Magnetic Phase Change in UO_2, Phys. Rev. **141**, 517 (1966).

[22] B. A. Berg and T. Neuhaus, Multicanonical ensemble: A new approach to simulate first-order phase transitions, Phys. Rev. Lett. **68**, 9 (1992).

[23] J. Zierenberg, N. G. Fytas, and W. Janke, Parallel multicanonical study of the three-dimensional Blume-Capel model, Phys. Rev. E **91**, 032126 (2015).

[24] Multicanonical simulations were performed on an Nvidia Tesla K80 GPU using 26 624 workers assigned to independent replicas [36, 37].

[25] K. Binder and D. P. Landau, Finite-size scaling at first-order phase transitions, Phys. Rev. B **30**, 1477 (1984).

[26] K. Binder, Theory of first-order phase transitions, Reports on Progress in Physics **50**, 783 (1987).

[27] J. Lee and J. M. Kosterlitz, New numerical method to study phase transitions, Phys. Rev. Lett. **65**, 137 (1990).

[28] J. Lee and J. M. Kosterlitz, Finite-size scaling and Monte Carlo simulations of first-order phase transitions, Phys. Rev. B **43**, 3265 (1991).

[29] D. Mataragkas, A. Vasilopoulos, N. G. Fytas, and D.-H. Kim, Tricriticality and finite-size scaling in the triangular Blume-Capel ferromagnet, Phys. Rev. Res. **7**, 013214 (2025).

[30] M. S. S. Challa, D. P. Landau, and K. Binder, Finite-size effects at temperature-driven first-order transitions, Phys. Rev. B **34**, 1841 (1986).

[31] W. Janke and R. Villanova, Three-dimensional 3-state Potts model revisited with new techniques, Nuclear Physics B **489**, 679 (1997).

[32] D. Merlini and C. Gruber, Spin-1/2 lattice system: Group structure and duality relation, J. Math. Phys. **13**, 1814 (1972).

[33] M. E. J. Newman and G. T. Barkema, *Monte Carlo Methods in Statistical Physics* (Oxford University Press, Oxford, 1999).

[34] L. N. Jorge, L. S. Ferreira, and A. A. Caparica, On the order of the phase transition in the spin-1 Baxter–Wu model, Physica A **542**, 123417 (2020).

[35] W. H. Press, S. A. Teukolsky, W. T. Vetterling, and B. P. Flannery, *Numerical Recipes in C* (Cambridge university press Cambridge, 1992).

[36] J. Zierenberg, M. Marenz, and W. Janke, Scaling properties of a parallel implementation of the multicanonical algorithm, Comput. Phys. Commun. **184**, 1155 (2013).

[37] J. Gross, J. Zierenberg, M. Weigel, and W. Janke, Massively parallel multicanonical simulations, Comput. Phys. Commun. **224**, 387 (2018).